Bamboo and Wood Structures

journal homepage: https://www.innoviair.cn/journal/BWS

Carbon-Negative and Lightweight: Engineered Bamboo Sandwich Panels for Sustainable Construction

Dingwu Huang[a,*]

[a]*Tianjin University of Urban Construction, Tianjin 3000384, China*

ARTICLEINFO

Keywords:
Bamboo Sandwich Panels
Grid Core
Four-Point Bending
Specific Strength
Sustainable Construction

ABSTRACT

This study developed a lightweight laminated bamboo sandwich panel (BSP) with a grid core, using bamboo veneers for both the surface and core layers. The effects of key structural parameters—including core processing methods, grid count, and layer thickness—on ultimate load capacity, deflection, strain, specific stiffness, and specific strength were systematically evaluated via four-point bending tests. Experimental results demonstrated that the core processing method significantly influences mechanical performance. Partition-type sandwich panels exhibited a 108.9% higher specific strength than interlocked-type panels. Increasing the number of long grids enhanced the ultimate load capacity by 68.4% and specific strength by 41.7%, whereas the number of short grids had a minimal impact. Reducing the lower layer thickness from 8 mm to 4 mm decreased specific strength by 24.2%, and decreasing the core thickness from 48 mm to 32 mm resulted in a 31.2% reduction. Nonlinear load-deflection and load-strain behaviors were observed, and a finite element simulation model successfully predicted the structural performance. Compared to traditional construction materials, the developed BSP offers superior structural efficiency, reduced environmental impact, and lower cost, demonstrating high potential for applications such as flooring, wall panels, and bridge decks.

1. Introduction

Rapid urbanization has led to unprecedented demand for infrastructure and building construction. However, this expansion has resulted in substantial depletion of natural resources and energy reserves, imposing a significant environmental burden globally. In response, sustainable development has become a critical strategic imperative. Adopting eco-friendly construction materials—thereby reducing reliance on conventional materials such as steel and concrete—represents a fundamental shift toward meeting sustainability objectives[1].

Bamboo, a historically utilized construction material, possesses remarkable properties including a high strength-to-weight ratio, superior mechanical characteristics, excellent structural plasticity, and inherent durability. These qualities position it as an ideal material for contemporary sustainable architecture[2]. Furthermore, the wider adoption of bamboo-based materials could alleviate anthropogenic pressure on diminishing natural forests in developing countries, thereby contributing to global conservation efforts.

As a significant non-timber forest product, bamboo is distinguished by its sophisticated fibrous architecture, favorable physicochemical properties, and good workability, making it a compelling alternative to conventional steel and concrete[3,4]. Its rapid growth cycle, notable ecological adaptability, and substantial socioeconomic benefits contribute to carbon sequestration and environmental amelioration throughout its life cycle. From a holistic life-cycle perspective, bamboo represents a premium eco-compatible material with broad application potential, aligning well with global and national sustainability goals such as China's dual carbon targets[5].

* Corresponding author.
E-mail addresses:huangdingwu@tcu.edu.cn
Received 20 September 2025; Received in revised form 30 September 2025; Accepted 15 November 2025; Available online 28 November 2025

In the context of bamboo's sustainability credentials, sandwich panel technology presents an innovative paradigm for maximizing its performance. Sandwich structures, known for their exceptional stiffness-to-mass ratios, have demonstrated remarkable versatility across aerospace, marine, and architectural applications[6-11].

Transforming laminated bamboo into grid-core sandwich structures offers opportunities to replace conventional floor and bridge deck components while providing a more environmentally sustainable alternative for the construction sector. This innovative application not only reduces the environmental footprint of building materials but also expands the potential uses of bamboo in construction, thereby accelerating the transition toward sustainable and ecological development (Fig 1).

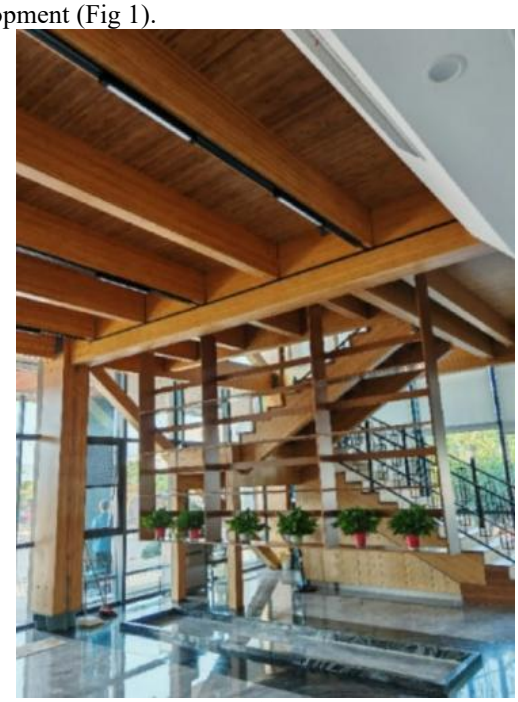

(a)

(b)

Fig 1. Modern bamboo and wood structure. a Laminated bamboo office building, b modern gluedlaminated timber footbridge

A sandwich panel typically comprises two thin, high-strength face sheets bonded to a lightweight core. This configuration enables optimized designs through the strategic selection of core topologies and face/core materials, thereby enhancing the mechanical properties of lightweight structures. Such designs yield superior multifunctional characteristics, including high stiffness-to-weight and strength-to-weight ratios, improved thermal insulation, and notable energy dissipation capacity. Driven by advances in high-specific-strength materials, sandwich structures have seen widespread adoption and diversification. Their structural performance depends critically on several factors: the properties of the face and core materials, the geometric configuration of the core, and the quality of the interfacial bond[12-16]. Consequently, tailoring face and core thicknesses along with core geometry provides a versatile pathway to meet diverse functional requirements. Researchers have proposed various core designs to develop lightweight structures with enhanced stiffness, strength, and energy absorption, with growing efforts focused on identifying optimal geometric configurations and material compositions for lightweight cores[17,18].

Grid structures, a class of sandwich core configurations, are generated by periodically extending basic structural units in two in-plane directions according to defined rules. Their cellular architecture consists of nodes interconnected by slender rod elements, resulting in various topologies such as triangular, honeycomb, square, and Kagome grids. Fan et al[19] fabricated carbon-fiber Kagome grid sandwich panels and subjected them to in-plane compression, out-of-plane compression, and three-point bending tests. Their experimental results were compared with theoretical predictions of bending failure modes, leading to refined theoretical models. He et al[20] derived theoretical formulas for the bending stiffness and strength of hexagonal grid sandwich panels made from low-carbon steel (Q235), with three-point bending tests showing close agreement with predictions. To enhance stiffness and mitigate interfacial mismatch, Shi et al[21] incorporated aramid fiber-reinforced honeycomb infill into square grid cores. Bending tests revealed that this infill improved the structure's strength, specific strength, and energy absorption capacity. Lu et al[22] employed 3D printing to design and fabricate quadrilateral, triangular, miter, and Kagome grid cores. Finite element analysis corroborated by three-point bending tests indicated that under bending loads, stress concentrations occurred in the upper face sheet beneath the loading zone and in the lower face sheet above the supports, while stress in the core concentrated between the loading and support zones. Failure modes varied: quadrilateral grids exhibited face-core interfacial delamination, whereas triangular, miter, and Kagome grids experienced core shear failure. Yang et al[23-25] designed and fabricated wood-based interlocking grid and pyramid sandwich structures, systematically evaluating their mechanical properties through flatwise compression and four-point bending tests. Their results indicated that the tension-dominated interlocking grid structure offered significant advantages over the bending-dominated pyramid structure, with compressive strength increasing by approximately 5.3 times, specific energy absorption by 79.6%, and bending stiffness by 5.5 times. Reinforcing OSB face sheets with glass fiber-reinforced

polymer (GFRP) increased flexural stiffness by 6.2–10.7% and transformed the failure mode from brittle fracture to stable plastic deformation. Klimek et al[26] developed a lightweight wood-based sandwich panel with a Kagome interlocking grid core and grooved particleboard facings, comprehensively determining its mechanical properties through systematic testing. The structure exhibited excellent performance in compression and bending, with flatwise compressive strength reaching 2.64 MPa, edgewise compressive strength 6.4 MPa, and flexural strength 10 MPa, though its tensile performance was relatively lower (average tensile strength of 0.5 MPa). The grooved connection system effectively enhanced interface stability, and Poisson's ratios measured via DIC technology provided crucial data for understanding the structural mechanical behavior. Hao et al[27] developed a novel wood-based Taiji honeycomb core sandwich panel and comprehensively analyzed its deformation and failure mechanisms under three-point bending through combined theoretical and experimental approaches. Their analysis showed that compared to traditional honeycomb cores, the Taiji honeycomb core exhibited 3.5 times and 3.44 times higher compressive and shear strength, respectively. In terms of strength-to-weight ratio, the compressive and shear strength increased by 1.75 times and 1.72 times, respectively. Indentation and core shear failure were identified as the primary failure mechanisms for these panels under three-point bending.

While considerable research has focused on the mechanical properties of sandwich panels, studies on laminated bamboo sandwich panels with grid cores (BSP) remain relatively scarce. Specifically, the flexural behavior and failure mechanisms of such structures are not yet fully understood. Therefore, this study designed and fabricated laminated bamboo grid sandwich panels with varying structural parameters. A combined approach of simulation analysis and bending tests was employed to rigorously investigate their flexural behavior and ascertain the underlying failure mechanisms. The findings are anticipated to provide crucial theoretical underpinnings for the practical engineering application of laminated bamboo grid sandwich panels, offering both significant engineering relevance and scientific value.

2.Experimental Methodology

This section details the test matrix, material properties, specimen manufacturing, test setup, and instrumentation.

2.1.Test Matrix

Sandwich panels with grid cores were fabricated from laminated bamboo, with dimensions of 1200 mm in length and 384 mm in width. All specimens were tested under four-point bending conditions and consisted of laminated bamboo face sheets bonded to both sides of the grid core. Two grid core processing methods were employed: interlocked and partition. The number of short grids varied among five levels: 3, 5, 7, 11, and 15, while the number of long grids was set to 3, 5, or 7. The lower face sheet thickness was 4 mm, 6 mm, or 8 mm, and the grid core thickness was 32 mm, 40 mm, or 48 mm. Three identical specimens were manufactured for each variable combination.

For identification, each specimen was labeled using a "BSP-XY" format, where "BSP" denotes laminated bamboo grid sandwich panel. "X" indicates the structural parameter category: interlocked triangular grid core (TI), interlocked square grid core (SI), interlocked Kagome grid core (KI), or partition square grid core (SP). "S" indicates the number of short grids; "L" the number of long grids; "T" the thickness of the lower face sheet (mm); and "H" the thickness of the grid core (mm). "Y" represents the specific value of the parameter.

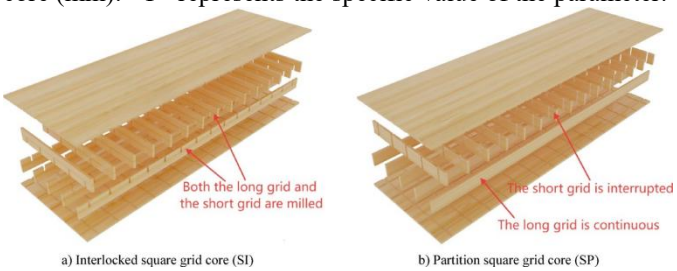

a) Interlocked square grid core (SI) b) Partition square grid core (SP)

Fig 2. Grid core of sandwich panel structure (a) Interlocked square grid core (SI) (b) Partition square grid core (SP)

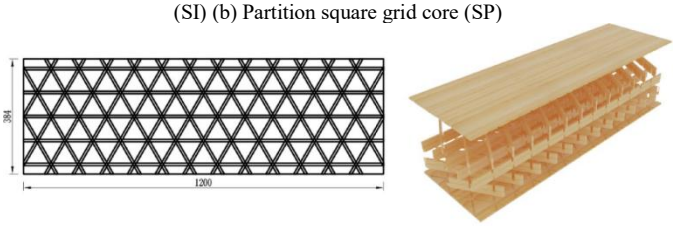

a) Laminated bamboo interlocked triangular grid sandwich panel (BSP-TI)

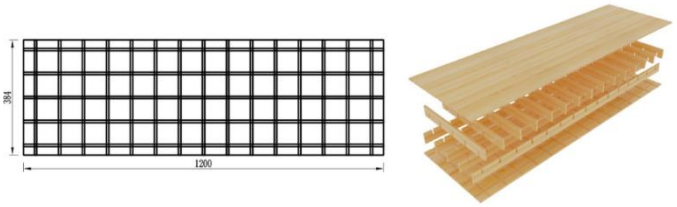

b) Laminated bamboo interlocked square grid sandwich panel (BSP-SI)

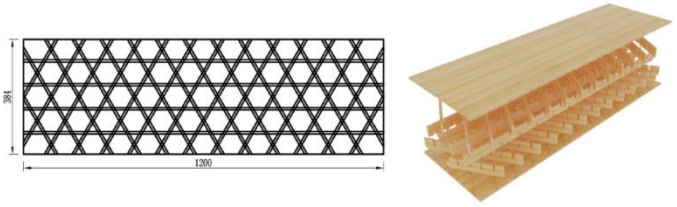

c) Laminated bamboo interlocked Kagome grid sandwich panel (BSP-KI)

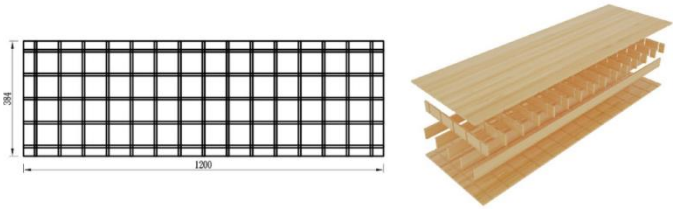

d) Laminated bamboo partition square grid sandwich panel (BSP-SP)

Fig 3. Engineered laminated bamboo sandwich panels

The length and width of the BSP were selected at a 1:1 scale based on typical bridge deck dimensions, while the height was determined according to the requirements of subsequent projects, considering the limitations of test fixtures, the stroke length of displacement transducers, and relevant specification requirements. Detailed structural parameters are

listed in Table 1, with geometric details illustrated in Figs 2 and 3.

Table 1 Geometric parameters of BSP

Specimen number	Core layer thickness (mm)	Lower surface layer thickness (mm)	Long grid quantity	Short grid quantity	Specimen quantity
BSP-TI	48	8	5	-	3
BSP-SI	48	8	5	15	3
BSP-KI	48	8	4	-	3
BSP-SP	48	8	5	15	3
BSP-S15	48	8	5	15	3
BSP-S11	48	8	5	11	3
BSP-S7	48	8	5	7	3
BSP-S5	48	8	5	5	3
BSP-S3	48	8	5	3	3
BSP-L7	48	8	7	7	3
BSP-L5	48	8	5	7	3
BSP-L3	48	8	3	7	3
BSP-T8	48	8	5	7	3
BSP-T6	48	6	5	7	3
BSP-T4	48	4	5	7	3
BSP-H48	48	4	5	7	3
BSP-H40	40	4	5	7	3
BSP-H32	32	4	5	7	3

2.2.Material Properties

The grid sandwich panels were manufactured from laminated bamboo. The laminated bamboo was supplied as single-layer boards measuring 2000 mm in length, 1500 mm in width, and with thicknesses ranging from 4 mm to 8 mm. The average density was 0.64 g/cm³. As an orthotropic material, its key mechanical parameters are listed in Table 2. To facilitate analysis of the BSP's mechanical behavior under four-point bending, a trilinear constitutive model (Fig 4) was implemented based on material test data.

A resorcinol adhesive with a viscosity of 15 Pa·s, procured from Shanghai Zhiyi New Material Technology Co, Ltd, was used to bond the face sheets to the core. To ensure optimal adhesion, the bonding surfaces of both the face sheets and the grid core were carefully polished. After adhesive application, the assembly was cured under cold-pressing conditions at 1 MPa pressure and 30 °C for 4 hours using a hydraulic press. This curing protocol ensured complete adhesive polymerization and produced robust interfacial adhesion, imparting the structure with excellent cohesion and durability.

Table 2 Basic properties of laminated bamboo

Material	Density ($g \cdot cm^{-3}$)	Tensile strength parallel to grain(MPa)	Compression strength parallel to grain(MPa)	Shear strength parallel to grain(MPa)
Laminated bamboo	0.64	114.5	59.7	18.9
Coefficient of variation/%	2.5	5.8	6.7	6.0

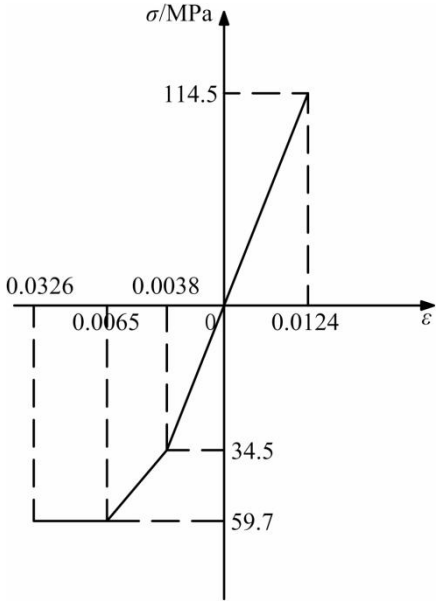

Fig 4. Constitutive model of laminated bamboo

2.3.Specimen Manufacturing

The BSP fabrication process is as follows, with the detailed structure shown in Fig 5.

First, laminated bamboo was precision-cut to the required dimensions for the face sheets and grid core. A computer numerical control (CNC) milling machine was then employed to mill specific grooves with high precision, efficiency, and repeatability. For the upper and lower face sheets, grooves with a depth of 3 mm were milled. For the triangular grid core, component 1–1 featured a groove depth equal to one-third of the laminated bamboo's width, while components 1–2 and 1–3 had grooves two-thirds of the width deep. For the square and Kagome grid cores, the groove depth was half the width of the laminated bamboo. Following the programmed path, the required grooves were accurately milled. The long and short grid ribs were then assembled using the interlocking method, where the grooves were carefully engaged to form a grid core with parallel upper and lower surfaces, ensuring a robust structure (Fig 6).

Resorcinol adhesive was uniformly applied to the grooves of the face sheets at a rate of 260 g/m² to ensure effective interfacial bonding. The grid core was positioned between the upper and lower face sheets to form the sandwich structure, with meticulous alignment maintained throughout assembly. The assembled panel was cold-pressed in a hydraulic press at 1 MPa and 30 °C for at least 4 hours to facilitate complete adhesive curing. After curing, the panel was trimmed to the final dimensions of 1200 mm × 384 mm using a cutting machine. Finally, the specimens were surface-finished with a fine sander to achieve a smooth texture, completing the fabrication process (Fig 7).

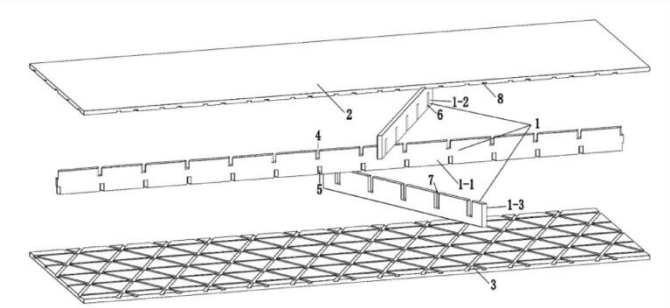

Fig 5. Details of laminated bamboo grid sandwich panel. Note: In this figure,1 represents the grid core, in which 1–1, 1–2 and 1–3 represent the middle, upper and lower layer of the grid core respectively. 2 represents the upper layer, 3 represents the lower layer, and 4 to 8 represent the groove positions between the grid core and the surface layer processed by the CNC milling machine

Fig 6. Interlocking and installing the grid core

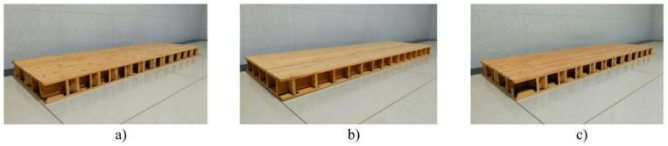

Fig 7. Laminated bamboo grid sandwich panel (a) Triangular grid (b) Square grid (c) Kagome grid

2.4.Test Procedure and Calculation Methodology

Four-point bending tests were conducted to characterize the mechanical behavior of all specimens. The loading and support spans were determined in accordance with established guidelines, specifically the Standard Test Methods for Timber Structures. A schematic of the four-point bending test setup is shown in Fig 8. Tensile strain on the lower surface and compressive strain on the upper surface were monitored using strain gauges attached to opposite sides of the BSP. Additionally, displacement transducers were positioned at mid-span and at the one-third points to measure structural deflection.

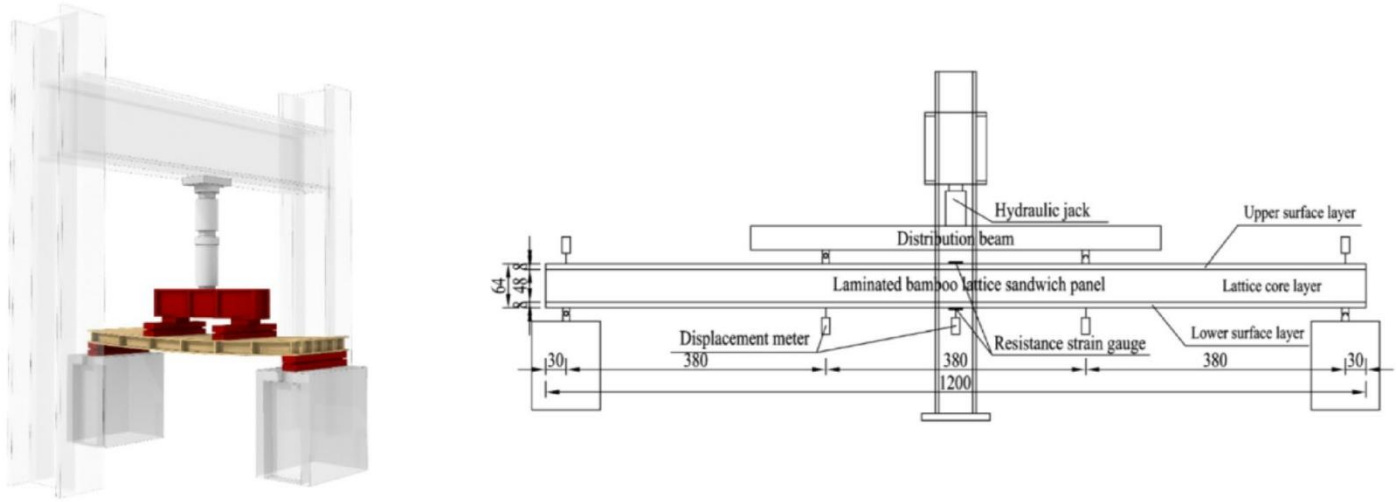

Fig 8. A schematic representation of the four-point bending test apparatus for BSP

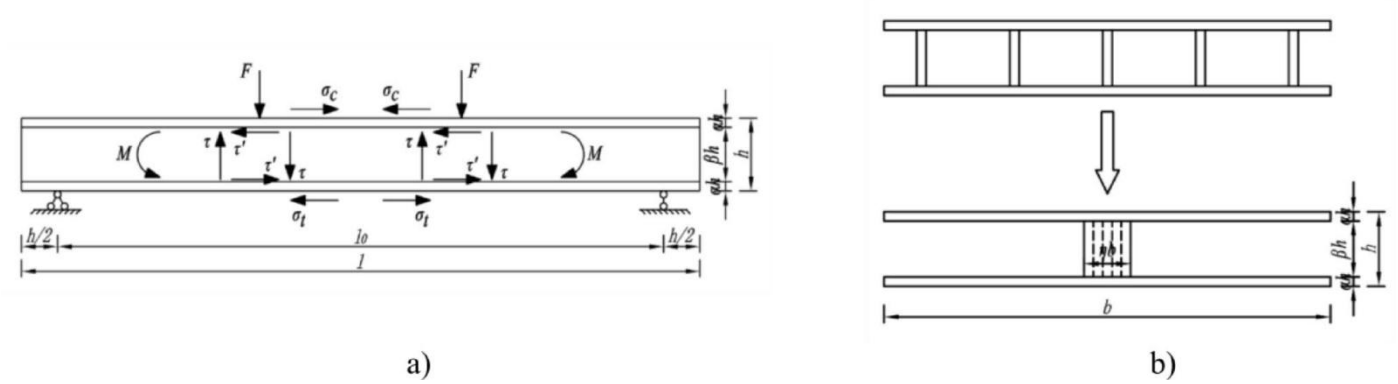

Fig 9. Section of laminated bamboo grid sandwich panel (a) Longitudinal section of BSP (b) Cross section of BSP

Testing was performed using a 10-tonne hydraulic actuator, with load applied incrementally at a constant rate. After each load increment, the load was held constant for three minutes, and readings were recorded once stabilization was achieved. This loading protocol continued until ultimate structural failure. The acquired data included load, deflection, and strain measurements.

The structural behavior of the BSP is analogous to that of an I-beam. As shown in Fig 9, the upper and lower face sheets function similarly to the flanges, resisting compressive and tensile stresses under bending, while the grid core acts like the web, resisting shear stresses. By placing the high-stiffness, high-strength face sheets farther from the neutral axis, the BSP configuration significantly enhances the overall bending stiffness.

In the figure, l represents the total length of the BSP (mm), l_0 denotes the calculated span (mm), b is the width (mm), and h is the total height (mm). The parameter η is the grid width coefficient, α is the face sheet thickness coefficient, and β is the grid core thickness coefficient.

$$\eta=\frac{b_{grid}}{b} \quad (1)$$

$$\alpha=\frac{h_{surface}}{h} \quad (2)$$

$$\beta=\frac{h_{grid}}{h} \quad (3)$$

Where b_{grid} is the width of the grid core, $h_{surface}$ is the thickness of the face sheet, and h_{core} is the thickness of the grid core.Namely, ηb refers to the width of the grid core (mm), αh indicates the thickness of the surface layer (mm), and βh represents the thickness of the grid core (mm).

Based on the principles of mechanics of materials, the bending moment M and shear force F_s acting on the cross-section can be related to the normal stresss σ and shear stress τ:

$$\sigma=\frac{My}{I_z} \quad (4)$$

$$\tau=\frac{F_s S_z^*}{I_z d} \quad (5)$$

Here, y is the distance from the neutral axis (mm), b is the width of the section considered for shear flow (mm), and I_z is the moment of inertia of the cross-section about the neutral axis z (mm⁴). S^*_z is the first moment of area of the section beyond the horizontal plane at distance y from the neutral axis z (mm³).

The expressions for I_z and S^*_z for the BSP are:

$$I_z=\frac{1}{2}bh^3[\alpha(1-\eta)\left(1-2\alpha+\frac{4\alpha^2}{3}\right)+\frac{\eta}{6} \quad (6)$$

$$S_z^*=\frac{1}{8}bh^2[4\alpha(1-\eta)(1+\alpha)+\eta \quad (7)$$

Let F_s and M_2 represent the shear force and bending moment, respectively, when the BSP reaches its ultimate shear strength. Similarly, let M_1 represent the bending moment when the structure reaches its ultimate tensile strength. The ultimate load-carrying capacity M is the smaller of M_1 and M_2:

$$F_s=2\tau bh^2[\frac{\alpha(1-\eta)(6-12\alpha+8\alpha^2)+\eta}{4\alpha(1-\eta)(1-\alpha)+\eta}] \quad (8)$$

$$M_1=\alpha bh^2[\alpha(1-\eta)\left(1-2\alpha+\frac{4\alpha^2}{3}\right)+\frac{\eta}{6} \quad (9)$$

$$M_2=\frac{2}{3}\tau bh^2[\frac{\alpha(1-\eta)(6-12\alpha+8\alpha^2)+\eta}{4\alpha(1-\eta)(1-\alpha)+\eta}] \quad (10)$$

$$M=\min\{M_1,M_2\} \quad (11)$$

Considering factors such as material quality, structural integrity, and potential strength variations, the strength values obtained from small, clear laminated bamboo specimens were adjusted using a reduction factor:

$$f_Q=K_Q f \quad (12)$$

$$K_Q=K_{Q1}K_{Q2}K_{Q3}K_{Q4} \quad (13)$$

Where f_q is the design material strength for the BSP (MPa), K_q is the comprehensive strength reduction factor, and f is the strength of small, clear laminated bamboo specimens (MPa). K_{Q1}, K_{Q2}, K_{Q3} and K_{Q4} are influence coefficients for natural defects, drying defects, long-term load effects, and size effects, respectively. Given the short loading duration in these tests, long-term effects were neglected. Due to strength reduction caused by milling and grooving, a natural defect impact coefficient for shear strength K_{Q1} = 0.78 was adopted. Other coefficients were assigned values in accordance with relevant standards.

3.Results and Discussion

This section details the failure modes, load-deflection and load-strain behaviors, and simulation results from the four-point bending tests. Finite element simulations using ABAQUS 2020 were conducted to elucidate the deformation behavior and stress distribution within the BSP.

The entire BSP was modeled using C3D8R hexahedral elements, a standard choice for simulating composite structures under bending. This element type employs reduced integration to mitigate shear locking while maintaining computational efficiency. The total element count ranged from 5,000 to 10,000, depending on the core geometry. A mesh sensitivity analysis was performed by refining the global element size from 20 mm to 5 mm. Results indicated that an 8 mm element size produced a mid-span displacement deviation of less than 2% compared to the finest mesh (5 mm), confirming result independence. This size was adopted for all models to ensure accuracy without excessive computational cost. In the simulation, the load was applied at the one-third points, with model dimensions matching those of the physical specimens (Fig 10).

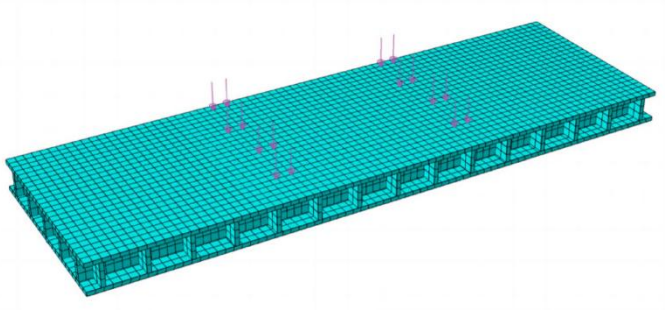

Fig 10. Finite element model of four-point bending test

3.1.Test Process and Analysis

3.1.1.Effect of Processing Method and Grid Core Configuration

This section examines the impact of two fabrication techniques (interlocked and partition) and three grid core geometries (triangular, square, Kagome) on the flexural behavior of BSP. The failure modes observed during four-point bending tests are shown in Fig 11. Test results are summarized in Table 3.

Under flexural loading, the stress distribution was as follows: the upper face sheet experienced compression, the grid core primarily resisted transverse shear, and the lower face sheet was in tension. Initially, no visible damage occurred. As the load reached approximately 65% of the ultimate load, the structure exhibited brittle behavior without significant surface cracking. At the ultimate load, a sudden loud noise was heard. Specimens fabricated using the interlocked method developed shear cracks within the bending shear zone, which propagated rapidly. Structural failure ensued when the grid core reached its ultimate shear strength. With continued loading post-peak, the laminated bamboo in the upper face sheet yielded upon reaching its compressive yield strength, while the lower face sheet failed in tension upon reaching its tensile strength.

The failure load was defined as the maximum load at the onset of damage, with the corresponding maximum displacement recorded. Representative load-midspan displacement and load-strain curves for each specimen group are compared with simulation results in Fig 12.

The curves show excellent agreement in slope during the elastic stage between experimental and finite element results. Upon entering the elastoplastic stage, the slopes decreased, but the overall trends remained broadly consistent with experimental observations.

The results indicate that grid core configuration and processing method significantly influence the ultimate load capacity. Among the interlocked specimens, the triangular grid core demonstrated the highest ultimate load and bending stiffness, followed by the Kagome and square grids. Compared to the square grid, the maximum loads of the triangular and Kagome grids increased by 71.9% and 22.2%, respectively. The partition-type square grid BSP showed a marked increase in maximum load—108.9% higher than the interlocked square grid and 21.6% higher than the interlocked triangular grid. However, bending stiffness showed no significant variation between square grid sandwich panels processed by different methods.

To quantitatively assess the impact of structural parameters, the specific stiffness and specific strength were calculated for each specimen group (Fig 13). Bending stiffness D was determined using:

$$D=\frac{a\cdot\Delta P}{48f_1}(3l^2-4\alpha^2) \quad (14)$$

where D is the bending stiffness (N·mm²), a is the distance from the support to the load point (mm), ΔP is the load increment within the elastic regime (N), l is the span (mm), and f_1 is the mid-span deflection (mm) corresponding to ΔP.The ratio $\Delta P/f1$ (N/mm) characterizes the linear segment of the load-displacement curve.

Among the interlocked BSP with different grid cores, BSP-SI exhibited the highest specific stiffness. The specific stiffness of BSP-TI and BSP-KI was slightly lower, at 95.2% and 92.8% of BSP-SI, respectively. The specific stiffness of square grid panels was largely unaffected by the processing method (partition vs. interlocked).

Regarding specific strength, BSP-TI (interlocked) showed the highest value among interlocked types. Notably, the specific strength of partition-type square grid panels (BSP-SP) was significantly enhanced—43.6%, 108.9%, and 95.3% higher than BSP-TI, BSP-SI, and BSP-KI, respectively. This suggests that the partition method enables more efficient material utilization for square grid sandwich panels.

Fig 11. Failure modes of BSP under bending loads (a) BSP-TI (b) BSP-SI (c) BSP-KI (d) BSP-SP

Table 3 Evaluation of test and simulation values for BSP

Specimen number	Test value		Simulation value		Relative error	
	Ultimate load (kN) ①	Mid-span displacement (mm) ②	Ultimate load (kN) ③	Mid-span displacement (mm) ④	Ultimate load ⑤=|①-③|/①	Mid-span displacement ⑥=|②-④|/②
BSP-TI	38.7	25.144	38.5	25.245	0.5%	0.4%
BSP-SI	22.5	14.731	23.5	15.322	4.4%	4.0%
BSP-KI	27.5	16.793	27.0	16.956	1.9%	1.0%
BSP-SP	47.0	41.991	46.9	41.198	0.2%	1.9%

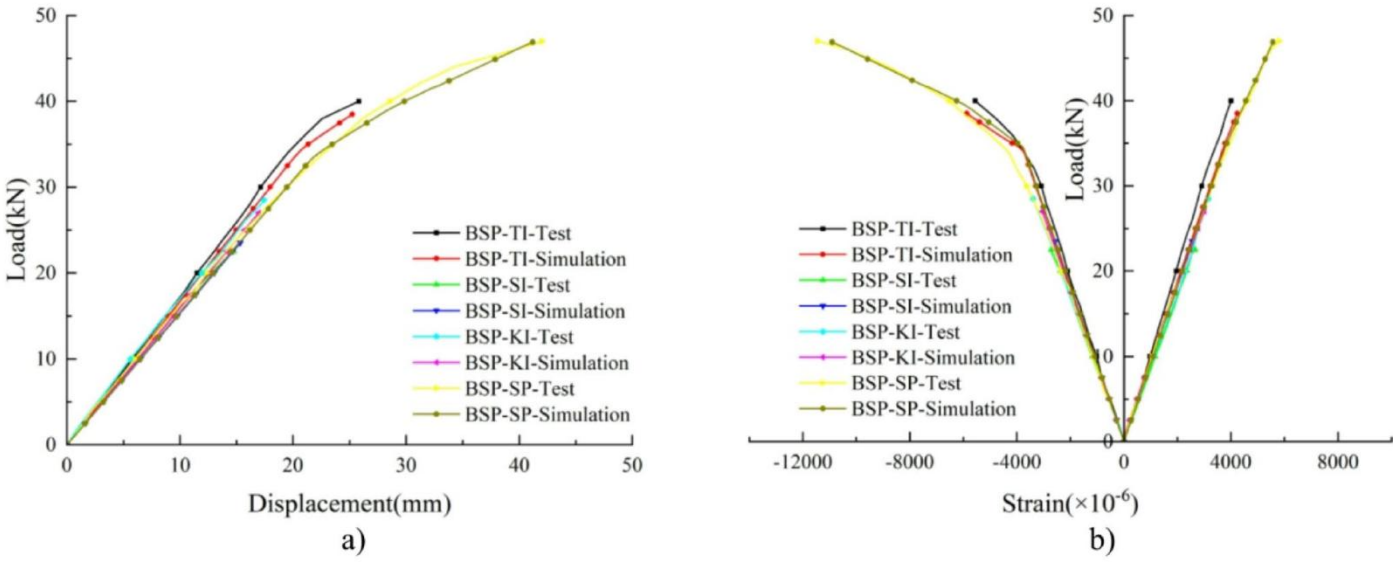

Fig 12. Comparison between test value and simulation value for BSP (a) Load-mid span displacement curve (b) Load-strain curve

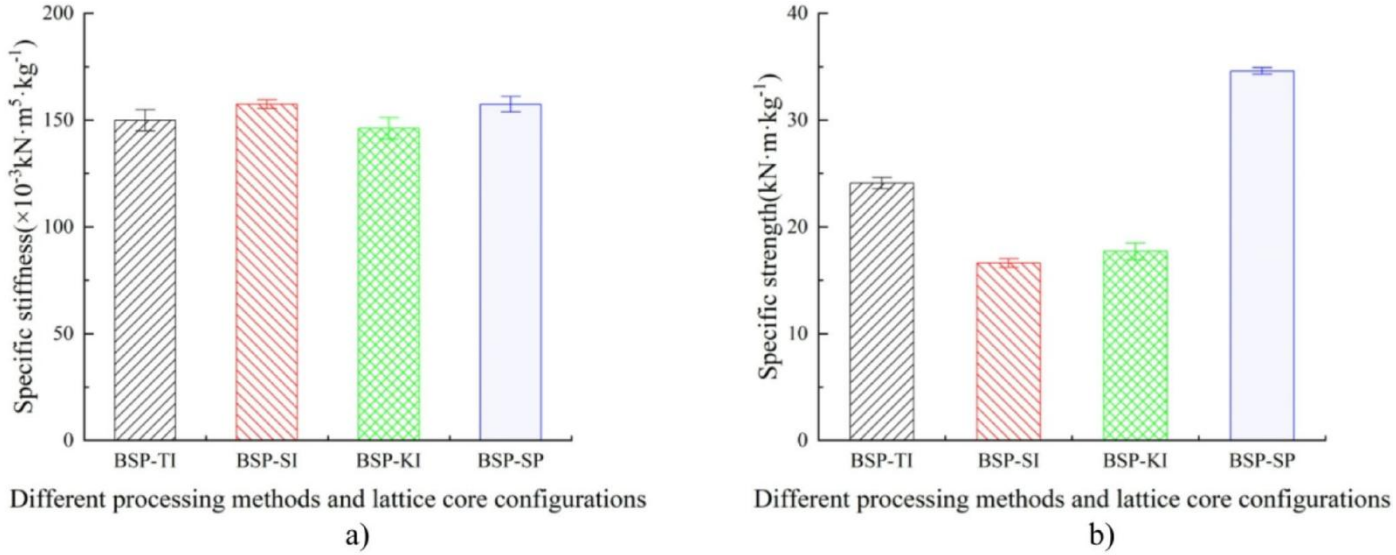

Fig 13. Specific stiffness and specific strength of BSP (a) Specific stiffness of BSP (b) Specific strength of BSP

3.1.2.Effect of Short Grid Quantity

This section investigates the relationship between the number of short grids and bending performance. Five structural groups were tested under similar conditions. The failure mode is illustrated in Fig 14, and results are summarized in Table 4.

Initially, specimens behaved elastically. As load increased, they transitioned into plastic deformation. Failure at the ultimate load was rapid. While ultimate load values across the five groups showed negligible variation, failure modes differed: BSP-S15, BSP-S11, and BSP-S3 exhibited tensile failure of the lower face sheet, whereas BSP-S7 and BSP-S5 failed due to shear in the grid core. This indicates that the number of short grids has minimal influence on the ultimate load capacity.

Load, deflection, and strain measurements are compared with simulation results in Fig 15.

The load-displacement curves for the five BSP groups with different short grid counts were similar, with nearly identical stiffness and ultimate load capacities. Among them, BSP-S15 had the highest ultimate load, measuring 1.011, 1.056, 1.056, and 1.044 times the values for BSP-S11, BSP-S5, BSP-S7, and BSP-S3, respectively.

Specific stiffness and specific strength are presented in Fig 16.

A clear trend emerged: as the number of short grids (and thus structural mass) decreased, both specific stiffness and specific strength increased. BSP-S3 exhibited the highest values, with specific stiffness and specific strength 24.9% and 12.5% higher than those of BSP-S15, respectively.

Fig 14. Failure modes of BSP under bending loads (a) BSP-S15 (b) BSP-S11 (c) BSP-S7 (d) BSP-S5 (e) BSP-S3

Table 4 Evaluation of test and simulation values for BSP

Specimen number	Test value		Simulation value		Relative error	
	Ultimate load (kN) ①	Mid-span displacement (mm) ②	Ultimate load (kN) ③	Mid-span displacement (mm) ④	Ultimate load ⑤=|①-③|/①	Mid-span displacement ⑥=|②-④|/②
BSP-S15	47.0	41.991	46.9	41.198	0.2%	1.9%
BSP-S11	46.5	41.264	46.9	41.483	0.9%	0.5%
BSP-S7	45.0	40.677	46.4	41.419	3.1%	1.8%
BSP-S5	44.5	39.541	45.9	40.604	3.2%	2.7%
BSP-S3	45.0	40.450	45.4	39.904	0.9%	1.4%

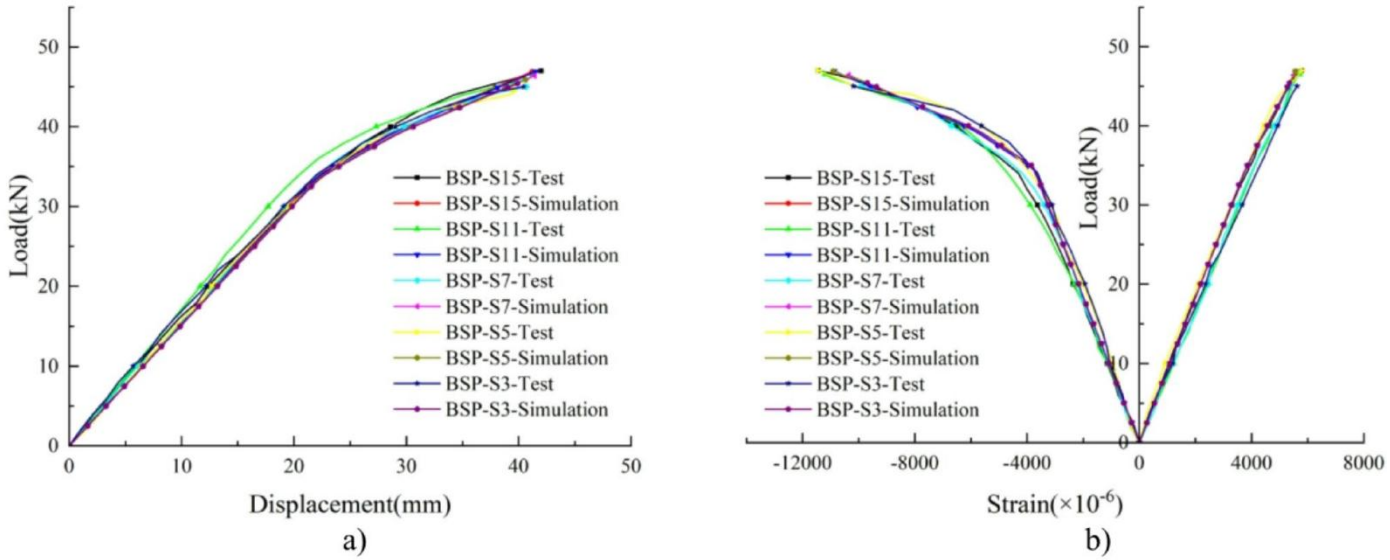

Fig 15. Comparison between test value and simulation value for BSP (a) Load-mid span displacement curve (b) Load-strain curve

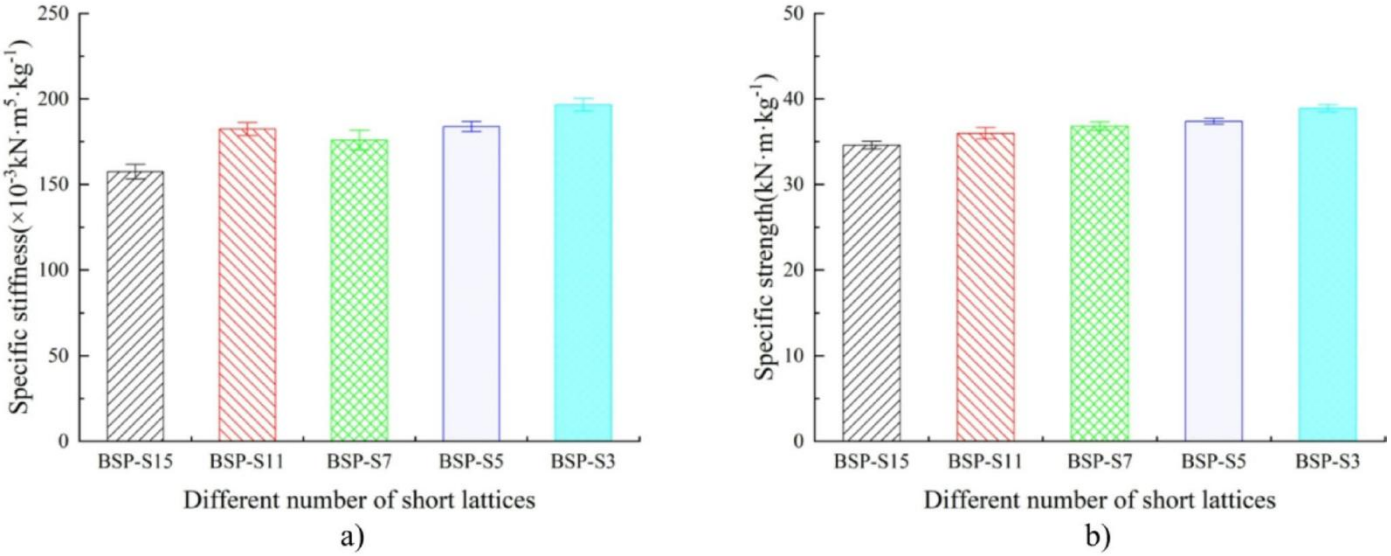

Fig 16. Specific stiffness and specific strength of BSP (a) Specific stiffness of BSP (b) Specific strength of BSP

3.1.3.Effect of Long Grid Quantity

This section examines the relationship between the number of long grids and flexural response. Three configurations were tested under comparable conditions. Failure modes are shown in Fig 17, and results are summarized in Table 5.

The loading behavior of the three configurations was similar, but failure modes differed: BSP-L3 remained primarily elastic, BSP-L5 transitioned gradually to plastic deformation, and both ultimately failed in shear as the grid core reached its shear strength. In contrast, BSP-L7 exhibited cracking in the lower face sheet after entering the plastic stage, culminating in tensile failure. This underscores the significant impact of long grid quantity on ultimate load capacity and failure mode.

Experimental data are compared with simulations in Fig 18.

Load-displacement curves showed similar initial elastic responses. However, BSP-L3, with inferior shear resistance, reached its ultimate capacity first, followed by BSP-L5 and BSP-L7.

Specific stiffness and specific strength are shown in Fig. 19.

A reduction in long grid number led to a modest decrease in specific stiffness: BSP-L5 and BSP-L3 were 2.2% and

8.0% lower than BSP-L7, respectively. While long grid quantity affected overall stiffness, the effect was relatively small. In terms of specific strength, BSP-L7 and BSP-L5 showed similar values, both substantially higher (41.7% and 44.3%, respectively) than BSP-L3. These findings indicate that the number of long grids significantly influences flexural performance. Increasing the number up to an optimal point enhances material utilization and structural performance.

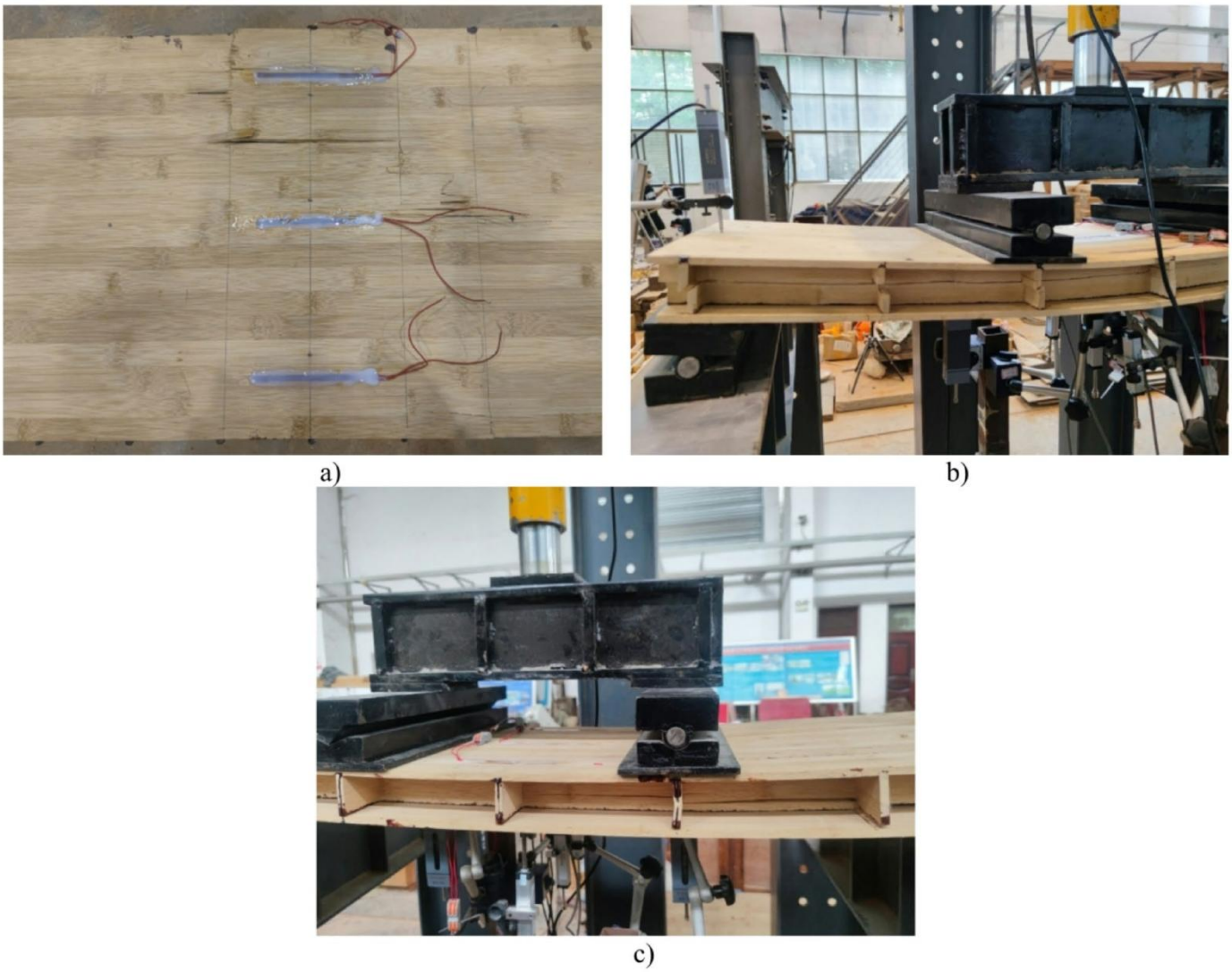

Fig 17. Specific stiffness and specific strength of BSP (a) Specific stiffness of BSP (b) Specific strength of BSP

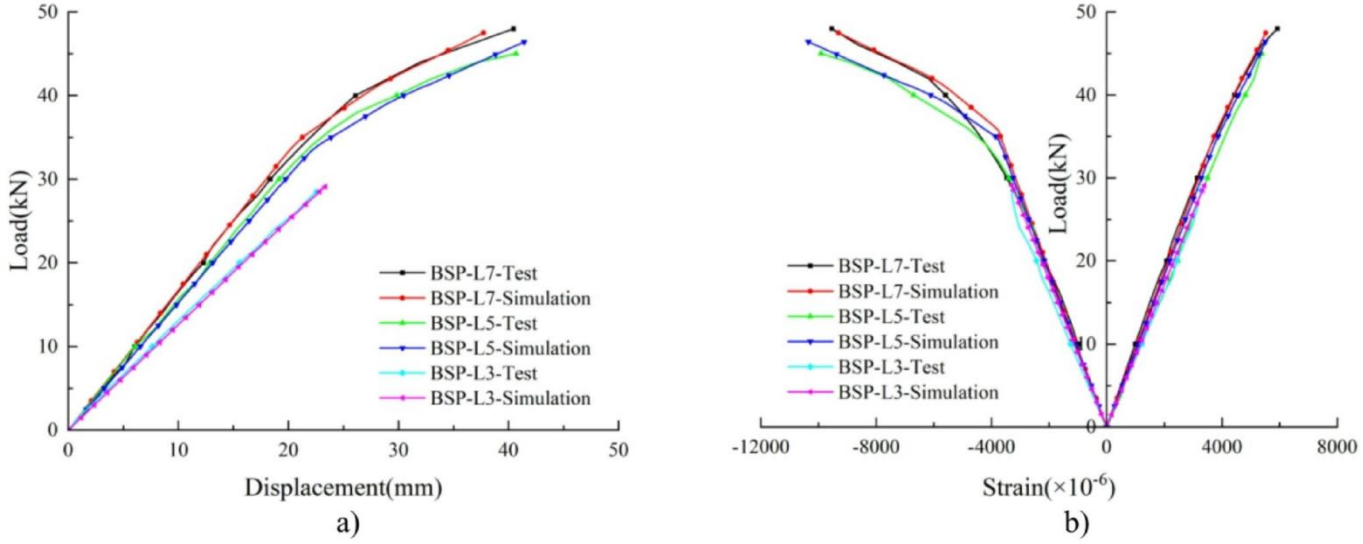

Fig 18. Comparison between test value and simulation value for BSP (a) Load-mid span displacement curve (b) Load-strain curve

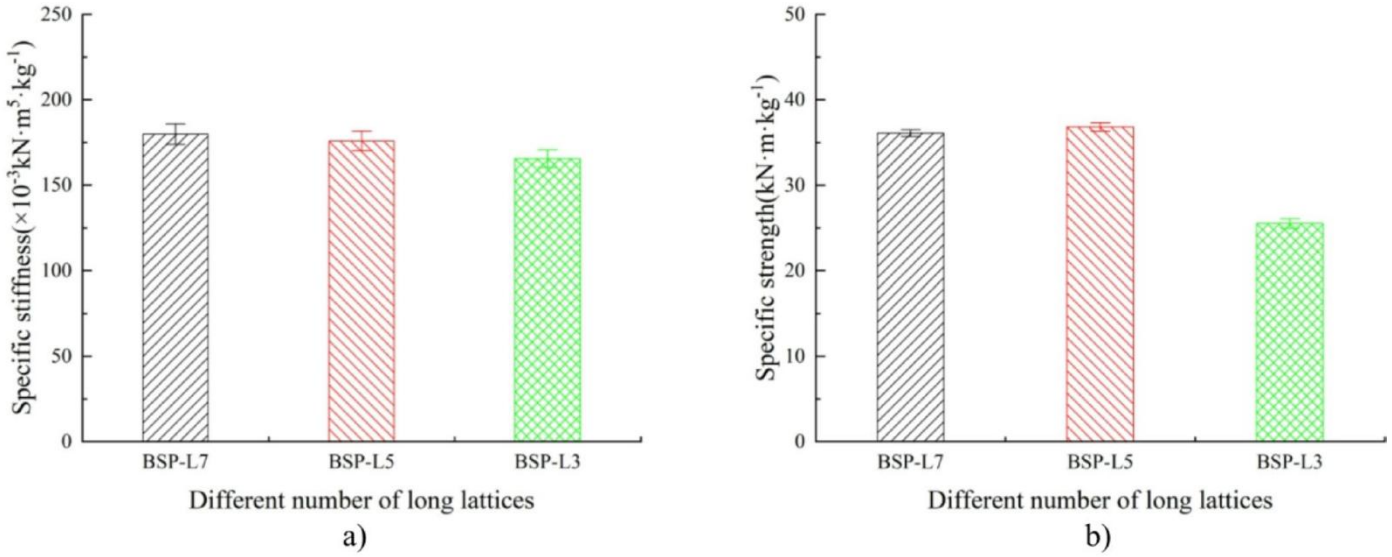

Fig 19. Comparison between test value and simulation value for BSP (a) Load-mid span displacement curve (b) Load-strain curve

Table 5 Evaluation of test and simulation values for BSP

Specimen number	Test value		Simulation value		Relative error	
	Ultimate load (kN) ①	Mid-span displacement (mm) ②	Ultimate load (kN) ③	Mid-span displacement (mm) ④	Ultimate load ⑤=|①-③|/①	Mid-span displacement ⑥=|②-④|/②
BSP-L7	48.0	40.454	47.5	37.731	1.0%	6.7%
BSP-L5	45.0	40.677	46.4	41.419	3.1%	1.8%
BSP-L3	28.5	22.569	29.1	23.327	2.0%	3.4%

3.1.4.Effect of Lower Face Sheet Thickness

This section examines the correlation between lower face sheet thickness and flexural performance. All three groups exhibited similar behavioral patterns. Characteristic failure modes are shown in Fig 20, and results are summarized in Table 6.

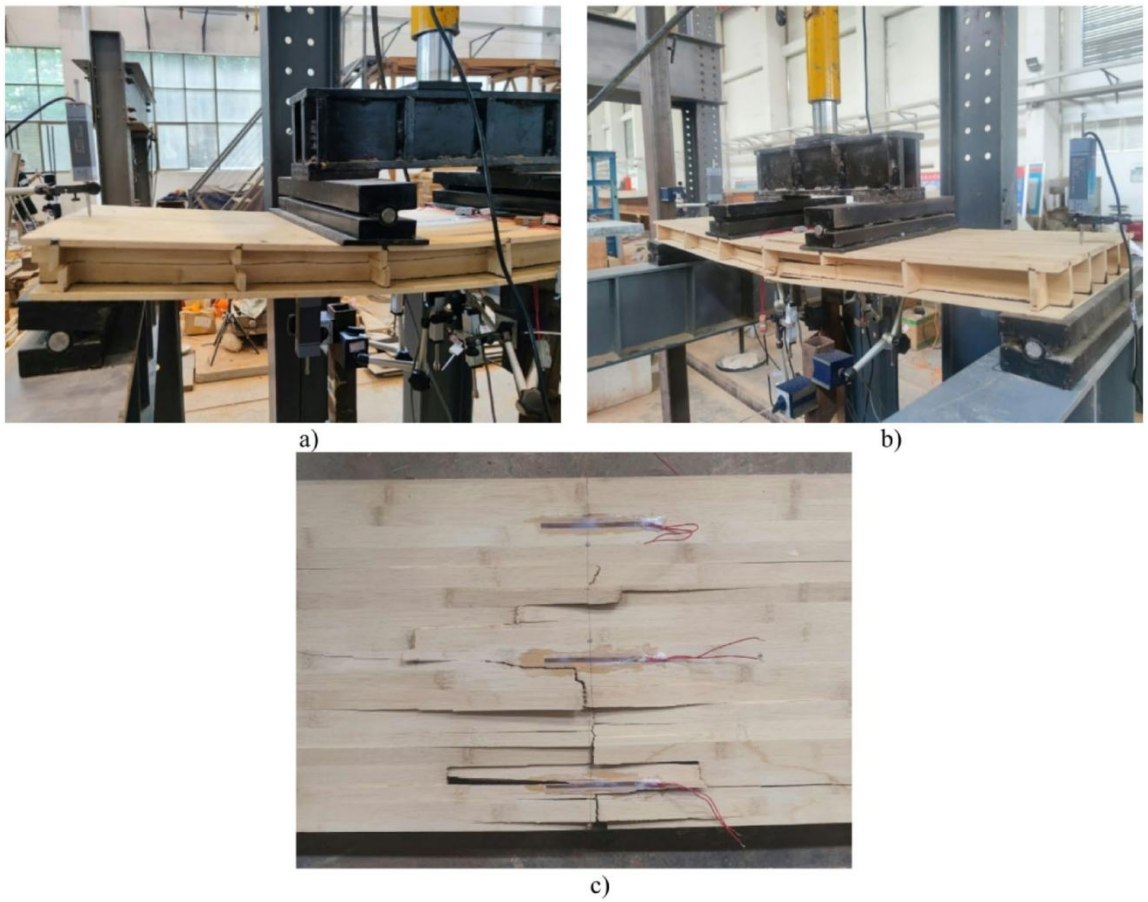

Fig 20. Failure modes of BSP under bending loads (a) BSP-T8 (b) BSP-T6 (c) BSP-T4

Table 6 Evaluation of test and simulation values for BSP

Specimen number	Test value		Simulation value		Relative error	
	Ultimate load (kN) ①	Mid-span displacement (mm) ②	Ultimate load (kN) ③	Mid-span displacement (mm) ④	Ultimate load ⑤=|①-③|/①	Mid-span displacement ⑥=|②-④|/②
BSP-T8	45.0	40.677	46.4	41.419	3.1%	1.8%
BSP-T6	36.0	30.443	38.0	33.121	5.4%	8.8%
BSP-T4	30.0	27.166	29.0	27.252	3.4%	0.3%

Although BSP-T8 and BSP-T6 had comparable ultimate loads, the variation in lower layer thickness (and thus total panel height) led to different failure mechanisms. BSP-T8 failed due to core shear, while BSP-T6 and BSP-T4 failed due to tensile failure of the lower face sheet. This demonstrates that lower face sheet thickness is a critical parameter governing both flexural performance and failure mode.

Experimental data are compared with simulations in Fig 21.

Load-deflection curves showed progressively shallower slopes with decreasing lower layer thickness. The 4 mm configuration (BSP-T4) failed in the elastic regime, while the 6 mm and 8 mm configurations (BSP-T6, BSP-T8) transitioned through elasticity before failing in the plastic domain. Reducing the thickness from 8 mm to 6 mm and 4 mm led to substantial reductions in ultimate load capacity of 20.0% and 33.3%, respectively.

Specific stiffness and specific strength are shown in Fig 22.

Specific stiffness was similar for BSP-T8 and BSP-T6, but BSP-T4 showed a notable reduction of 12.9%. Specific strength decreased by 12.5% for BSP-T6 and 19.5% for BSP-T4 compared to BSP-T8. These findings demonstrate that increased lower face sheet thickness correlates with enhanced flexural performance and material utilization efficiency.

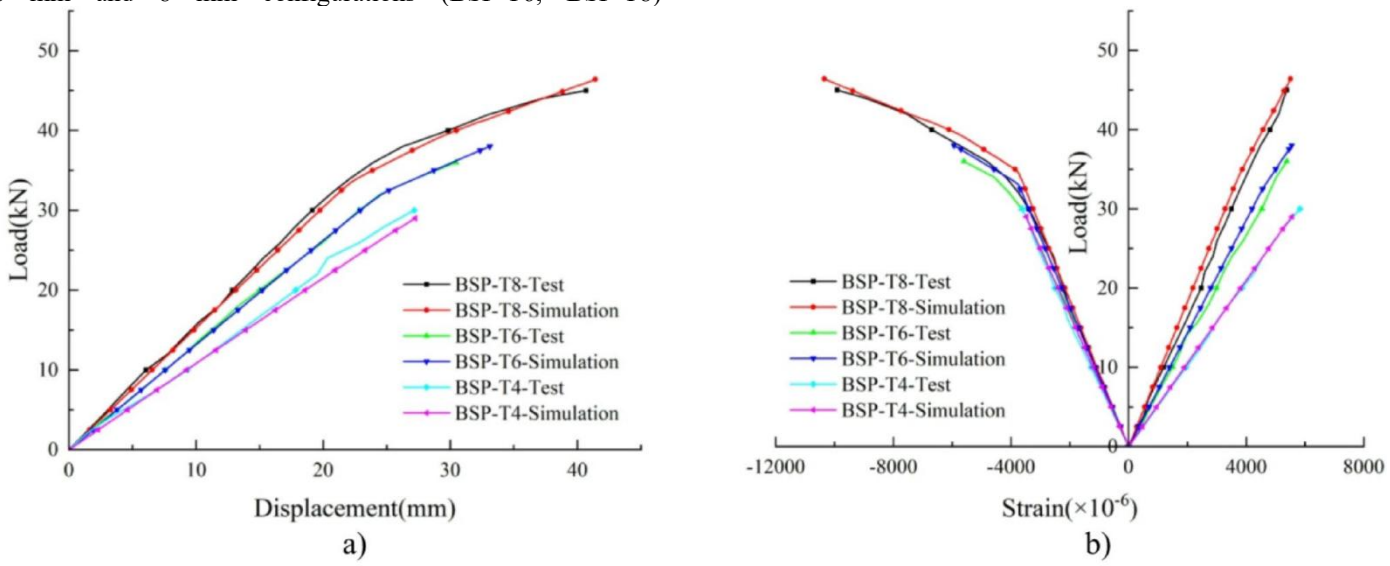

Fig 21. Comparison between test value and simulation value for BSP (a) Load-mid span displacement curve (b) Load-strain curve

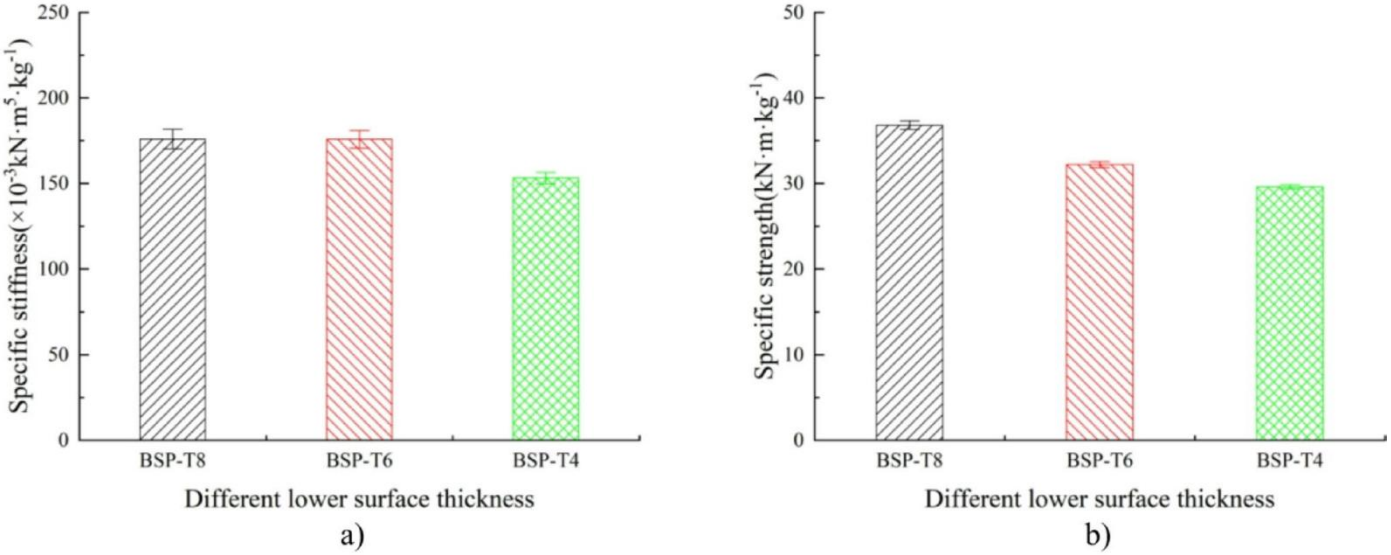

Fig 22. Specific stiffness and specific strength of BSP (a) Specific stiffness of BSP (b) Specific strength of BSP

3.1.5.Effect of Grid Core Thickness

This section investigates the relationship between grid core thickness and flexural performance. All three configurations exhibited tensile failure, but variations in core height led to

significant differences in ultimate load capacity. Failure modes are shown in Fig 23, and results are summarized in Table 7.

A direct correlation was observed: increased grid core thickness enhanced the ultimate load capacity, underscoring its critical role in determining flexural performance. Greater core height contributes to superior stiffness and strength.

Experimental data are compared with simulations in Fig 24.

Load-displacement curves were predominantly linear until failure for all three groups. As grid core thickness decreased, structural stiffness and ultimate load capacity declined. BSP-H40 and BSP-H32 retained 68.6% and 57.1% of the ultimate load of BSP-H48, respectively. Failure in all cases was attributed to tensile fracture of the lower face sheet.

Specific stiffness and specific strength are shown in Fig 25.

Both specific stiffness and specific strength diminished markedly with reduced grid core thickness. Compared to BSP-H48, BSP-H40 showed reductions of 25.4% and 26.8% in specific stiffness and strength, respectively, while BSP-H32 showed more pronounced reductions of 43.9% and 34.7%.

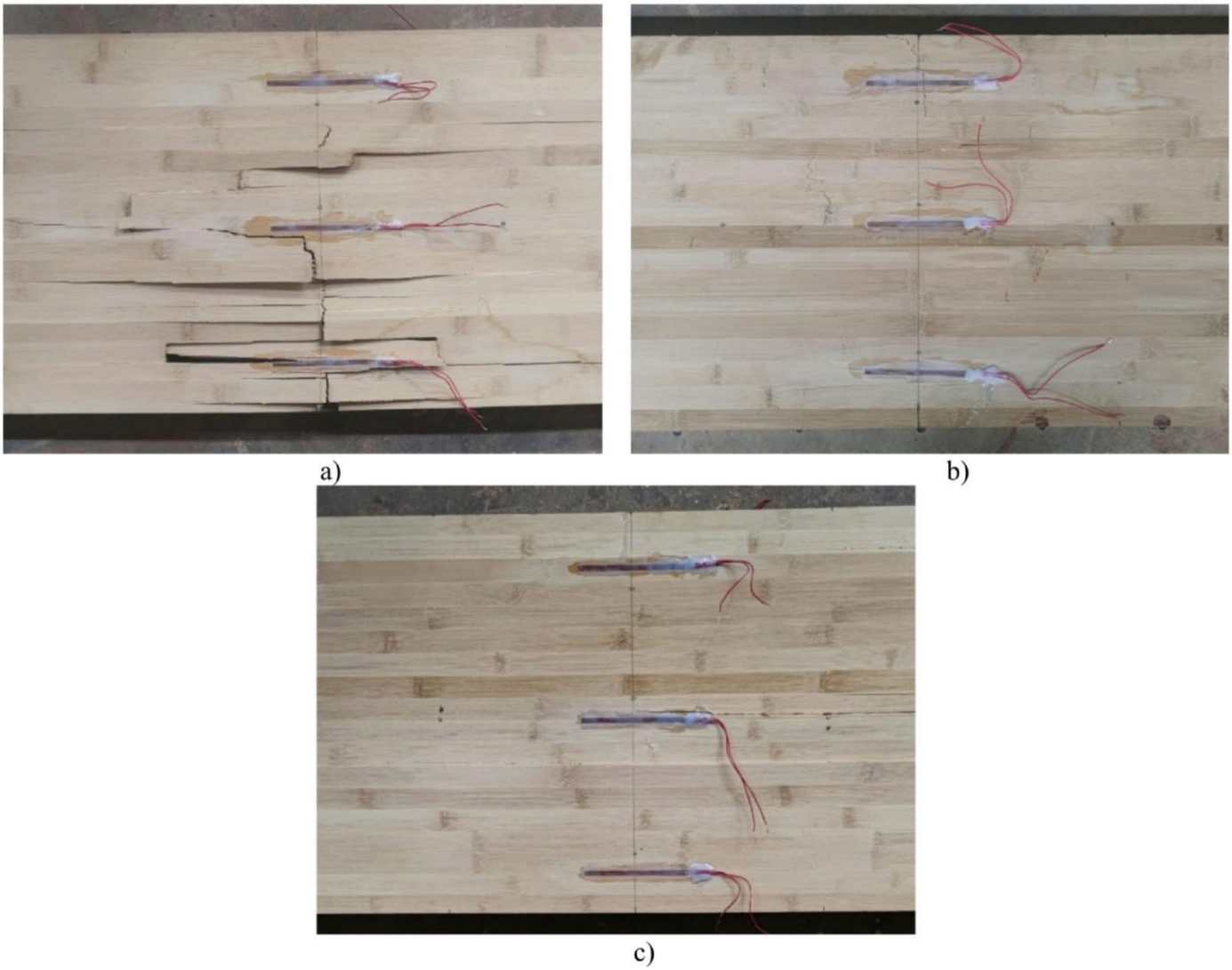

Fig 23. Failure modes of BSP under bending loads (a) BSP-H48 (b) BSP-H40 (c) BSP-H32

Table 7 Evaluation of test and simulation values for BSP

Specimen number	Test value		Simulation value		Relative error	
	Ultimate load (kN) ①	Mid-span displacement (mm) ②	Ultimate load (kN) ③	Mid-span displacement (mm) ④	Ultimate load ⑤=|①-③|/①	Mid-span displacement ⑥=|②-④|/②
BSP-H48	45.0	40.677	46.4	41.419	3.1%	1.8%
BSP-H40	36.0	30.443	38.0	33.121	5.4%	8.8%
BSP-H32	30.0	27.166	29.0	27.252	3.4%	0.3%

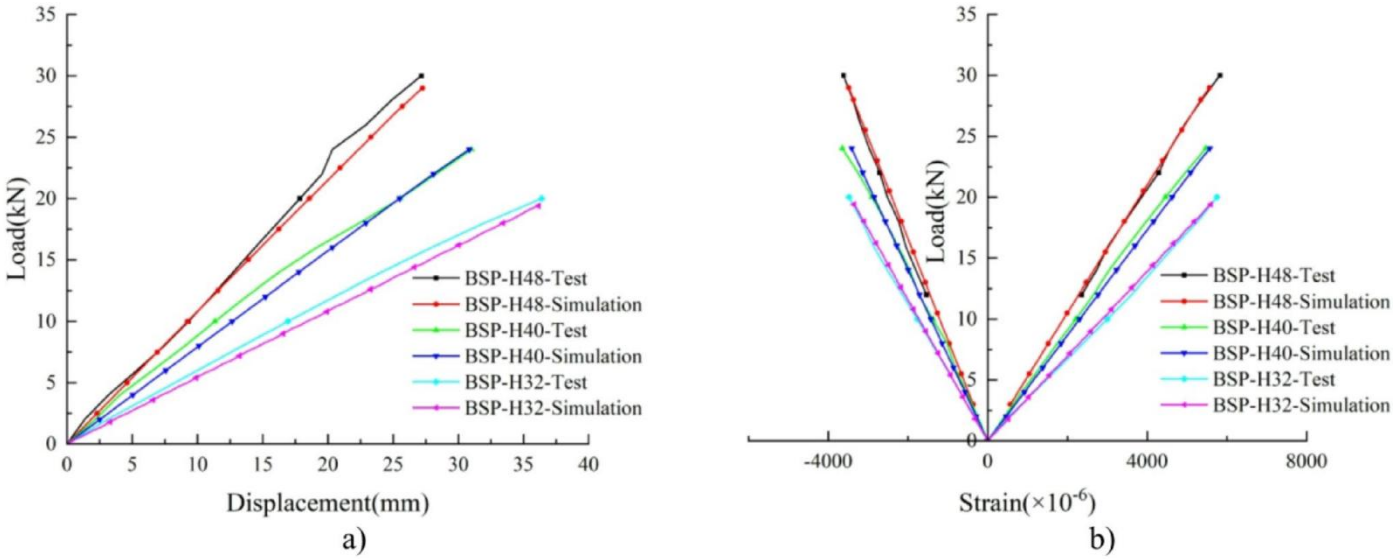

Fig 24. Comparison between test value and simulation value for BSP (a) Load-mid span displacement curve (b) Load-strain curve

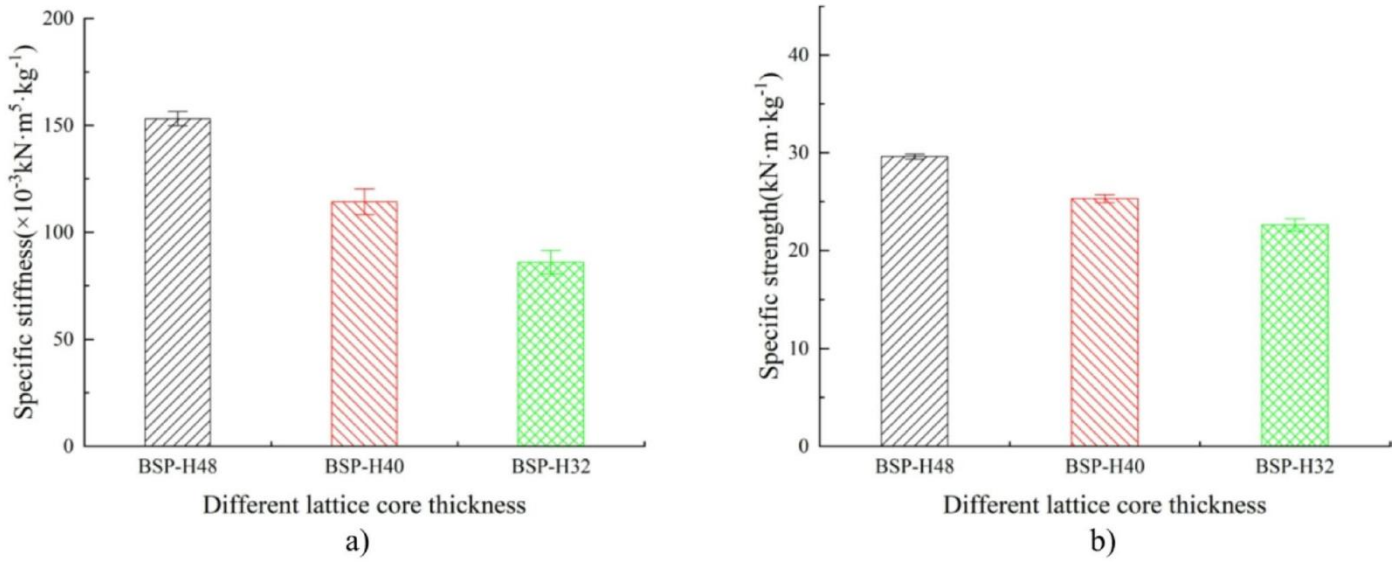

Fig 25. Specific stiffness and specific strength of BSP (a) Specific stiffness of BSP (b) Specific strength of BSP

3.2.Parametric Study

The flexural capacity of each specimen group was calculated by substituting the corresponding BSP parameters into the derived formulas; results are presented in Table 8.

Table 8 Comparison between test value and theoretical value of BSP

Specimen number	Ultimate load-carrying capacity (kN·m)		Relative error ③=|①- ②|/①
	Test value ①	Theoretical value ②	
BSP-L3	5.4	5.4	0.4%
BSP-L5	8.6	8.9	3.8%
BSP-L7	9.1	8.6	6.2%
BSP-T4	5.7	5.1	10.3%
BSP-T6	6.8	6.7	1.4%
BSP-T8	8.6	8.9	3.8%
BSP-H32	3.8	3.3	13.5%
BSP-H40	4.6	4.2	8.8%
BSP-H48	5.7	5.1	10.3%

Experimental and theoretical values show strong correlation, with relative discrepancies within 15%. For BSP-L3, BSP-L5, BSP-L7, BSP-T6, and BSP-T8, deviations were predominantly within 5%, demonstrating the reliability of the theoretical approach for predicting ultimate load capacity. For BSP with equal upper and lower face sheet thicknesses, experimental findings indicate that specific strength is maximized with five long grids, a face sheet thickness of 8 mm, and a grid core thickness of 48 mm—a configuration that optimally leverages material properties. Based on these findings, further investigations explored the influence of various structural parameters.

3.2.1.Influence of Grid Core Width

The effect of grid core width was investigated by varying the width coefficient η (Fig 26).

When η is below a critical threshold, BSP failure is governed by the material's ultimate shear strength (core shear failure). When η exceeds this value, failure is controlled by the ultimate tensile strength. As η increases, ultimate load capacity also increases, but the rate of increase diminishes significantly beyond the critical threshold. In the shear-dominated region, specific strength increases with η; in the tension-dominated region, it declines. This trend suggests maximum specific strength occurs in the transitional region

between shear and tensile failure. Based on the analysis, an optimal grid core width of 38 mm is identified.

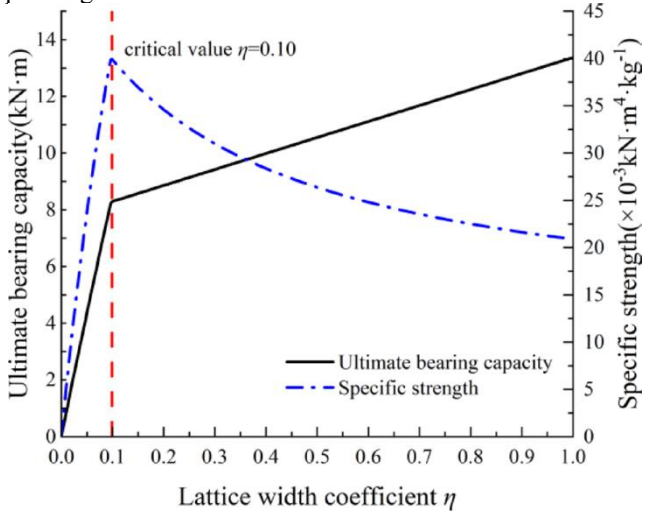

Fig 26. Influence of grid core width

3.2.2.Influence of Face Sheet Thickness

The influence of face sheet thickness was investigated by varying the coefficient α (Fig 27).

When α is below a critical value, failure is governed by tensile strength. Once α surpasses this value, failure transitions to shear strength control. As α increases, ultimate load capacity increases at an accelerating rate. In the tension-dominated region, specific strength improves with increasing α; in the shear-dominated region, it declines. Peak specific strength occurs in the transitional region. The optimal face sheet thickness is determined to be 8 mm.

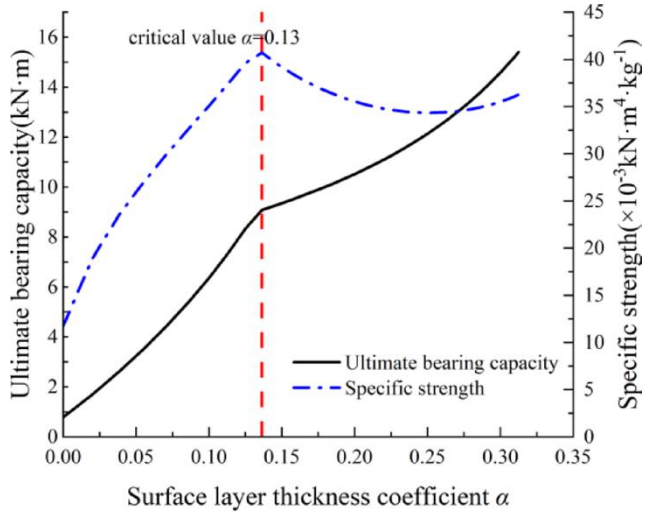

Fig 27. Influence of surface layer thickness

3.2.3.Influence of Grid Core Thickness

The effect of grid core thickness was examined by varying the coefficient β (Fig 28).

When β is below a critical value, failure is shear-dominated; above it, failure is tension-dominated. Ultimate load capacity increases with β, with a more pronounced rate in the shear-dominated region. Specific strength increases with β in the shear-dominated region but decreases in the tension-dominated region, peaking at the transition. The optimal grid core thickness is identified as 62 mm.

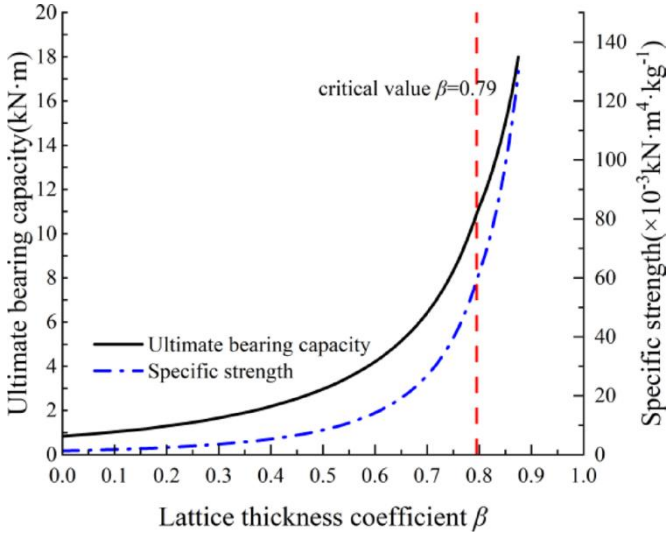

Fig 28. Influence of grid core thickness

3.2.4.Influence of Height-to-Span Ratio

The influence of the overall structural height-to-span ratio h/l was also analyzed (Fig 29).

When h/l is below a critical threshold, failure is shear-dominated, with both ultimate load capacity and specific strength increasing as h/l decreases. When h/l exceeds the critical value, failure is tension-dominated, and both metrics remain relatively invariant. Optimal performance is achieved when the height-to-span ratio is maintained below 1/18.

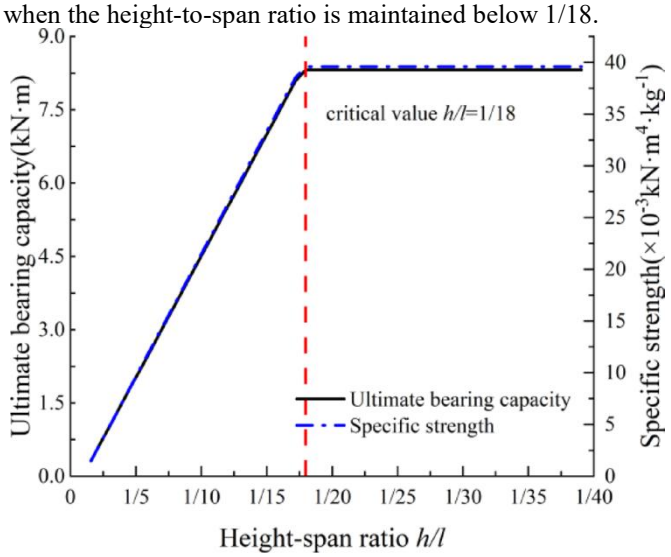

Fig 29. Influence of structural height-span ratio

4.Conclusions

This study developed an innovative laminated bamboo grid sandwich panel (BSP) and fabricated a series of specimens with varying structural parameters. Their bending performance was investigated through four-point bending tests. Based on the empirical data, a theoretical formula for calculating the load-carrying capacity of BSP was formulated and compared with experimental results. A finite element model was constructed in ABAQUS to perform a nonlinear analysis, which was benchmarked against experimental findings. The main conclusions are as follows:

(1) Grid configuration and fabrication method profoundly influence the bending performance of BSP. Among the three

interlocked grid types studied, the triangular grid exhibited the highest specific strength, surpassing the square and Kagome grids by 45.5% and 36.0%, respectively. The partition-type square grid panel demonstrated markedly superior ultimate load capacity and specific strength compared to the interlocked triangular grid, with enhancements of 21.6% and 43.6%, respectively, indicating optimal utilization of bamboo's material properties. The quantity of short grids has a negligible impact on flexural performance, whereas the number of long grids significantly modulates structural behavior. Reducing the thickness of the lower face sheet and the grid core leads to a concomitant decrease in ultimate load capacity and specific strength. Increasing the number of long grids from three to seven enhanced ultimate load capacity and specific strength by 68.4% and 41.7%, respectively. Reducing the lower face sheet thickness from 8 mm to 4 mm decreased specific strength by 24.2%, while reducing the grid core thickness from 48 mm to 32 mm resulted in a 31.2% decline.

(2) A theoretical formula for the load-carrying capacity of BSP was derived. The calculated values show good agreement with experimental results, with relative errors not exceeding 15%. Through comparative analysis of flexural capacity and specific strength under varying parameters, and considering structural cost, material utilization, and performance, the optimal cross-sectional configuration for BSP was identified: a grid core width of 38 mm, face sheet thickness of 8 mm, grid core thickness of 62 mm, and a height-to-span ratio below 1/18. Increasing the three key parameters—grid core width, face sheet thickness, and grid core thickness—enhances the ultimate load capacity and specific strength of BSP. However, beyond critical thresholds related to tensile and shear failure, the failure mode transitions. Concurrently, specific strength diminishes with increases in grid core width and face sheet thickness beyond their optimal points, while both ultimate load capacity and specific strength increase with a reduction in the height-to-span ratio below its critical value.

(3) The ABAQUS finite element model showed high consistency with experimental results. The simulated flexural capacity matched test values with errors primarily within 5% (maximum 8.8%). Trends in mid-span displacement and strain distribution aligned closely with experiments. The model confirmed the failure modes: tensile failure in the lower face sheet at mid-span within the bending zone, and shear failure near the neutral axis of the grid core in the bending-shear section, validating experimental observations.

References

[1] CHANG F C, CHEN K S, YANG P Y, KO C H. Environmental Benefit of Utilizing Bamboo Material Based on Life Cycle Assessment. Journal of Cleaner Production, 2018, 204: 60–69.

[2] FLANDER K D, ROVERS R. One Laminated Bamboo-frame House per Hectare per Year. Construction and Building Materials, 2009, 23: 210–218.

[3] LI Z H, CHEN C J, MI R Y, et al. A Strong, Tough, and Scalable Structural Material from Fast-Growing Bamboo. Advanced Materials, 2020, 32: 1906308.

[4] WANG X D, JIAO L A, DU Y S, et al. Experiment and Design Approach of Steel-to-Laminated Bamboo Lumber Screwed Connections Under Load Parallel to Grain. Journal of Cleaner Production, 2022, 380: 134964.

[5] QING Y. Advanced Functional Materials Derived from Natural Wood and Bamboo Resources Under the Double Carbon Strategy in China. Journal of Central South University of Forestry & Technology, 2022, 42: 13–25.

[6] WEI P, CHEN J, ZHANG Y, PU L. Wood-based Sandwich Panels: A Review. Wood Research, 2021, 66: 875–890.

[7] OLIVEIRA P R, MAY M, PANZERA T H, HIERMAIER S. Bio-based/Green Sandwich Structures: A Review. Thin-Walled Structures, 2022, 177: 109426.

[8] ANSELL M P. Hybrid Wood Composites – Integration of Wood with Other Engineering Materials//WOOD COMPOSITES. Amsterdam, Netherlands: Elsevier, 2015: 411–426.

[9] CASTANIÉ B, PEIGNON A, MARC C, et al. Wood and Plywood as Eco-materials for Sustainable Mobility: A Review. Composite Structures, 2024, 329: 117790.

[10] GUENTHER R, TAJMAR M, BACH C. Wood and Wood-Based Materials in Space Applications—A Literature Review of Use Cases, Challenges and Potential. Aerospace, 2024, 11: 910.

[11] PALOMBA G, EPASTO G, CRUPI V. Lightweight Sandwich Structures for Marine Applications: A Review. Mechanics of Advanced Materials and Structures, 2022, 29: 4839–4864.

[12] MANALO A C, ARAVINTHAN T, KARUNASENA W. Flexural Behaviour of Glue-laminated Fibre Composite Sandwich Beams. Composite Structures, 2010, 92: 2703–2711.

[13] LUO Y M, ZHENG Y, LI R. Experimental Research on Flexural Behavior of FRP Sandwich Panels with Hybrid Core. Industrial Construction, 2020, 50(3): 167–171.

[14] PELIŃSKI K, SMARDZEWSKI J. Bending Behavior of Lightweight Wood-Based Sandwich Beams with Auxetic Cellular Core. Polymers, 2020, 12: 1723.

[15] WANG Z, YANG X L, LAI W G, et al. A VAM-Based Equivalent Model for Triangular Honeycomb Sandwich Panels: Comparison with Numerical and Experimental Data. Materials, 2022, 15: 4766.

[16] WANG Z, ZHOU L, ZHANG Z, MWAMBALA M A. Study on Bending Performance of Laminated Bamboo Sandwich Panels with Different Lattice Core Layers: Cleaner Production of Green Material. Case Studies in Construction Materials, 2024, 20: e03379.

[17] ASHBY M F. The Properties of Foams and Lattices. Philosophical Transactions of the Royal Society A: Mathematical, Physical and Engineering Sciences, 2006, 364: 15–30.

[18] WANG Z F, ZHOU L C. Bending Performance of Laminated Bamboo Sandwich Panels with Different Lattice Cores. Journal of Beijing Forestry University, 2025, 47(1): 147–155.

[19] FAN H L, MENG F H, YANG W. Sandwich Panels with Kagome Lattice Cores Reinforced by Carbon Fibers. Composite Structures, 2007, 81: 533–539.

[20] HE M F, HU W B. A Study on Composite Honeycomb Sandwich Panel Structure. Materials & Design, 2008, 29: 709–713.

[21] SHI S S, SUN Z, HU X Z, CHEN H. Flexural Strength and Energy Absorption of Carbon-fiber–Aluminum-honeycomb Composite Sandwich Reinforced by Aluminum Grid. Thin-Walled Structures, 2014, 84: 416–422.

[22] LU C, QI M X, ISLAM S, et al. Mechanical Performance of 3D-printing Plastic Honeycomb Sandwich Structure. International Journal of Precision Engineering and Manufacturing-Green Technology, 2018, 5: 47–54.

[23] YANG D, FAN C S. The Mechanical Properties of Wood-Based Grid Sandwich Structures. Forests, 2022, 13: 877.

[24] YANG D X, FAN C S, DING B R, et al. Mechanical Behavior of Lightweight Wood-Based Interlocking Grid Sandwich Cell Structure. Forest Engineering, 2023, 39(1): 92–100.

[25] YANG D, GUO L, FAN C. Flexural Performance and Failure Mode of Wood-Based Sandwich Structure Plate Members. BioResources, 2025, 20: 6522–6546.

[26] KLÍMEK P, WIMMER R, BRABEC M, SEBERA V. Novel Sandwich Panel with Interlocking Plywood Kagome Lattice Core and Grooved Particleboard Facings. BioResources, 2015, 11: 195–208.

[27] HAO J X, WU X F, OPORTO G, et al. Deformation and Failure Behavior of Wooden Sandwich Composites with Taiji Honeycomb Core Under a Three-point Bending Test. Materials, 2018, 11: 2325.